13th World Conference on Earthquake Engineering
Vancouver, B.C., Canada
August 1-6, 2004
Paper No. 470

SUBSURFECE STRUCRTURE AND WAVEFORM MODELING IN THE NOBI PLAIN, JAPAN

Hideki Nagumo[1] and Yoshihiro Sawada [1]

SUMMARY

We construct the Nobi plain subsurface structure model based on geological survey results and check the validity of it. First, we conducted microtremor explorations near eastern boundary of the plain and determined S-wave structures in order to compensate the lack of the geophysical information. Together with our results and other geophysical survey results, we construct the Nobi plain subsurface structure model. Next we perform three-dimensional finite difference waveform modeling of two strong motions in the frequency range of 0.1 to 0.5 Hz observed in the Nobi plain during M5.5 and M4.7 earthquakes. Our simulation results reproduced overall features observed in seismic data at most stations. This agreement suggests the validity of the model.

INTRODUCTION

The Nobi plain has an area of about 1300 square kilometers and has a basin structure. Nagoya city, which is one of the largest cities in Japan, is on it and more than one million people are living here. The Nobi plain suffered severe damage during historical large earthquakes. Remarkable examples are the the 1891 Nobi earthquake (M8.0) and the 1944 Tonankai earthquake (M7.9). Recently occurrence of Tokai and/or Tonankai earthquakes is worried about. So it is important to capture the underground structure in terms of two or three dimension for seismic hazard assessment.

In the Nobi plain not so much geophysical surveys are conducted until recently. From 2001 to 2003 detail subsurface structure surveys, consist of reflection survey and microtremor survey, were conducted by Aichi Prefecture Government, which make it possible to consider wider range of the subsurface structure. Fig.1 shows geophysical survey locations conducted in the plain. Gravity survey, refraction survey, reflection survey, microtremor survey and PS logging is conducted. Most of the geophysical surveys are conducted in southern part of the plain. Three reflection lines are across the eastern plain boundary. Each reflection result showed the nearly same basement topography. Large offsets of 1.0 to 2.0 km between mountain area and sediments in the plain are recognized there. Other results conducted in the plain showed the basement beneath the plain inclines from north-east to south-west. On the other hand dense micrtremor explorations are conducted south part of the plain by Masaki [1]. In this area irregular shape of the basement are reported.

[1] Graduate School of Engineering, Nagoya University, Japan

After 1998 more than 60 seismic observation sites are set up in the Nobi plain by various organizations. Acceleration seismograph is installed at all sites. In this study we use seismic observation data for two earthquakes (M5.5 and M4.7) occurred around the Nobi plain. Fig.2 shows location of seismic observation sites and epicenters of two earthquakes. One is occurred in the west of the plain at a depth of 5 km and the other is occurred in the south-east of the plain at a depth of 51 km.

In this article we first estimate S-wave velocity structures near the eastern Nobi plain boundary by microtremor exploration method, because no geophysical survey is conducted in this area. Next the Nobi plain subsurface model is constructed based on these geophysical survey results. Finally we perform three-dimensional finite difference waveform modeling of strong motions in the frequency range of 0.1 to 0.5 Hz observed in the Nobi plain during M5.5 and M4.7 earthquakes.

THREE DIMENSIONAL SUBSURFAVE MODEL OF THE NOBI PLAIN

Microtremor array observations

Method

Fig.2 shows locations of our observations. ISS, NGK is located at the east part of the plain and the others are at the north-east part. In the observation we use UD component velocity seismometers with 5 sec natural period and recorder with 24bit A/D resolution and GPS time synchronization. Microtremor exploration process is shown in fig.3. A circular array consisting of four stations is used in measurements. At each site three measurements are conducted by different array size. Each size is determined by expected basement depth at each site shown in Table 1. Space and auto-correlation method (Aki [2]) is applied to the observed data and Rayleigh wave phase velocities are extracted. Finally we estimate S-wave structure using the genetic algorithm (Yamanaka [3]).

On the other hand, PS converted wave is clearly seen in observed seismic data at most sites on the plain during M5.5 event. This wave is considered to generate at the basement-sediment boundary just below the observation site. There are seismic observation sites near each microtremor sites and PS converted waves are clearly seen on the observed waveforms there (fig.4). The arrival time difference between P-wave and PS converted wave is different from site to site. This difference is considered to contain geophysical structure information beneath the site. Then we incorporate this time difference to the inversion process. We assume flat multi-layers and plane wave incidence, then PS-P time is expressed by following,

$$t_{PS-P} = \sum_{i=1}^{n} \eta_i \cdot h_i - \sum_{i=1}^{n} \xi_i \cdot h_i$$

where h_i , η_i and ξ_i means thickness and vertical slowness of S-wave and P-wave of i-th layer, respectively. We assume incident angle 66 degree and incorporate time difference in the calculation of misfit function defined by following.

$$misfit = \frac{1}{n} \sum_{i=1}^{n} \left| C_i^{obs} - C_i^{theo} \right| + \left| t_{PS-P}^{obs} - t_{PS-P}^{theo} \right|$$

where N is number of the observed phase velocity data and C is phase velocity. In the inversion process P-wave velocity and density corresponding to S waves are assumed using the empirical relation reported by Ludwig [4]. We assume 3 layers in the sediments based on other survey results conducted in the plain and fix basement S-wave velocity at 3.2 km/s. Each layer thickness and S-wave velocity is estimated by inversion.

Analysis and results

In 1999 we conducted microtremor explorations at east part of the plain. HYM and TRM are located about 2km and 5km westward from ISS. We also estimate S-wave structure at these two sites in this study. Fig.5 shows inversion results. At each site theoretical phase velocities are fit well to the observed ones. TRM and HYM are located near the refraction survey line. In fig. 6 basement depth estimated by refraction survey is also shown. Basement depths at TRM and HYM are nearly same between microtremor exploration results and reflection survey results. On the other hand, PS logging is conducted at NGK recently. At this site not only basement depth but also S-wave velocities in the sediments are fit well which indicate that validity of our experiments. At east 4 sites estimated S-wave velocity of each sedimentary layer is nearly same at each site. S-wave velocity is about 0.6km/s in the third layer and about 0.4km/s in the second layer. The reliability of S-wave velocity of the surface layer is considered to be not so high, because estimated S-wave velocity is lower than obtained Rayleigh wave phase velocities.
Basement is inclined from east to west on this line.

On the other hand, inversion results of north-east 3 sites are shown in fig.5. Estimated S-wave velocity of each sedimentary layer is also nearly same in neighboring sites, which is about 1.0 km in the third layer and about 0.6 km/s in the second layer. These S-wave velocities are a little higher than those at east part.

3D Nobi plain subsurface model

Based on these geophysical survey results we construct Nobi plain subsurface structure model. Modeled area is shown in fig.6, which covers the region 40km wide in the N334E direction, 60km long in the N66E direction. North-west part of the plain are excluded because of the lack of geophysical information and seismic data.

Basically results obtained by reflection survey and refraction survey provide line information and those by microtremor experiments and PS logging provide point information. Then we use gravity Bouguer anomaly information (Geophysical Survey of Japan, [5]) to connect geophysical survey results. Fig.7 shows contour map of basement, basement is inclined from north-east to south-west. We assume four layer sediments and thickness of each layer corresponding to the basement depth. P and S wave velocities at each layer are shown in table 2, which are average values of survey results.

As state before, during 1998 event PS converted wave are clearly seen at most sites during M5.5 event. We calculate PS-P arrival time difference using 1D structure of our model at each site and compare with observed result. Fig.8 shows the results. Observed PS-P time is long in the south-west part of the plain and gradually become shorter to the north-west. Calculated time reproduce observed pattern well.

3D SIMULATION

Simulation method

We use the fourth-order staggered grid finite difference method using discontinuous grid proposed by Aoi [6]. This method use two regions, one is consist of grids with fine spacing near the surface and the other is consist of grids with three times coarser in the deeper region, which result in a significant reduction of computational requirements. We also incorporate non-uniform grid spacing technique by Pitarka [7] along Z direction in deeper region.

We use stress free condition at free surface proposed by Graves [8] and non reflecting boundary condition by Ceijean [9] at the other boundaries. Attenuation effect by Q value is incorporated by Graves's [8] method.

Model

In this simulation model proposed before is divided by 0.l km spacing until 2.7 km depth. Lower portion of the model is divided by 0.3 km spacing. In the region deeper than 7.5 km, grid spacing changed to 1.0 km along only Z direction.

In the deeper part of the basin structure, we assume four crustal layers. P and S-wave velocities at each layer determined based on Ukawa [10] and each layer thickness is based on the refraction survey result by Aoki [11]. The lowest layer is correspond to the Phillipine see plate, which upper boundary is determined by Yamazaki [12]. The upper boundary of this layer is assumed to be inclined along N67E direction from 49 km to 59 km in depth. Geophysical parameters of each layer are shown in table 2.

In the two simulations we assume a double couple point source and a bell shaped source time function with a duration of 2 sec. We only compare waveform at observation sites inside the the Nobi plain because reliability of the model.

1998 4/22Event modeling

The location of this event is west of the plain and close to the plain. The epicentral distance is about 10km and source depth is 5km. We calculated velocity seismograms for a source with a focal mechanism of strike=24, dip=68, and dip=108 in degree. Fig.9 shows the observed and calculated velocity waveforms, band pass filtered from 0.1 to 0.5 Hz. We select 9 sites as a reference at each district of the plain shown in fig.10.

Amplitudes and waveforms of S-wave portion are well simulated at most sites. After S-wave portion, observed waveforms are complicated, having longer duration with many later arrivals. Our 3D simulation succeeds in reproducing both amplitudes and phases of the observed waveforms at most sites. However, our 3D model does not reproduce all of the details of the observed waveforms. For example, the well-developed later phases after S-wave on horizontal components are not reproduced at FNK, The well-developed later arrivals at 40 to 50 sec on the horizontal components at KTA are not reproduced by the 3D simulation. Though later phases with large amplitude are reproduced, timing is different at HYM. In this simulation fitting between observed and simulated waveforms are better at stations located in the west of the plain.

Fig. 11 shows band pass filtered (0.1-0.5 Hz) velocity waveforms at sites on the west-east line across the Nobi plain. The propagation of Raylegh wave generated at western edge of the plain is clearly seen in observation waveforms with the apparent velocity of about 0.5 km/s. In the simulation waveforms Rayleigh wave are also reproduced. However propagation velocity become slightly faster in the central part of the plain.

Results of 1999 11/29 Even

The location of this event is occurred in the opposite side (SW part of the plain) of M5.5 event. Source depth of this event is 51km. We calculated velocity seismograms for a source with a focal mechanism of strike=47, dip=78, and dip=133 in degree. Fig.12 shows the observed and calculated velocity waveforms, band pass filtered from 0.1 to 0.5 Hz.

In this event maximum amplitude are recorded in S-wave portion. Waveforms and amplitudes of S-wave portion are well simulated at most sites. Later phases with larger amplitude are also reproduced at most sites but amplitude of these phases is underestimated at some sites.

HYM is located on a hilly area near the eastern boundary of the plain. 13 seismographs are installed in approximately 1.3 by 0.8 km area. Using the observation and simulation data at HYM, we analyze the propagation characteristics of later phases and compared them. In the simulation array had 5 receivers arranged in a square pattern. We apply semblance method Neidell [13] to UD components for determination of propagation direction and phase velocity. The semblance value in a time window indicates coherence among the waveforms observed at stations in that window. In this study we use 2 sec time window. In fig.13 analysis results are shown. In the observation results semblance values of S wave portion are not so large. But after 5sec from S wave arrival semblance values become larger. In this portion apparent velocities are about 1.0 km/s and propagation directions are about N80E direction constantly. These phase velocities are corresponding to Rayleigh wave phase velocities around 0.5 Hz at HYM. This wave is considered to be basin induded Rayleigh wave generaged at the eastern boundary. On the other hand, in the simulation results, though propagation directions are slightly different, observed phase velocities and propagation directions are well reproduced.

CONCLUSION

We conducted microtremor explorations near eastern boundary of the plain and determined S-wave structures in order to compensate the lack of the geophysical information. We conclude that the microtremor exploration is a very promising method for determining S-wave structures from shallow to intermediate depths. After that we construct the Nobi plain subsurface structure model based on geophysical survey results. Calculated PS-P time using our model reproduces PS-P time at most sites during M5.5 event well.

Our simulations also reproduce generation and propagation of basin induced wave at western and eastern boundary of the plain. Gross pattern of amplification and duration in observed data are well reproduced. But waveform, timing and amplitude of arrival of later phases have a little difference at some sites. These results suggest that though overall feature of model is valid, we should need improvement in detail.

ACKNOLEDGEMENTS

In this study we used K-net and Kik-net strong motion records and PS logging results from NEID. We also used earthquake observation records by Aichi Prefecture Government, Mie Prefecture Government and Nagoya City Government and reflection survey results by Aichi Prefecture Government. Source parameters used are determined as earthquake mechanism analysis using broadband seismic waveforms conducted under Freesia Project from NEID. Elevation data by Geographical Survey Institute [14] were used to draw some of the maps. Several figures ere plotted with Generic Mapping Tools (GMT) by Wessel [15].

REFERENCES

1. Masaki, Kazuaki, Yoshihiro Sawada, Hideki Nagmo, Miyako Norita, Susumu, Kurahashi, and Suqun Ling (2004). “Earthquake observation using hot spring borehole and microtremor array survey in southwest part of Nagoya City”, submitting to 13 WCEE, Canada.
2. Aki, K. (1957). Space and time spectra of stationary stochastic waves, with special reference to microtremors, Bull. Earthq. Res. Inst. 35, 415-456.

3. Yamanaka, H. and H. Ishida (1996). Application of genetic algorithms to an inversion of surface-wave dispersion data, Bull. Seism. Soc. Am. 86, 436-444.
4. Ludwig, W. J., J. E. Nafe, and Drake (1970). Seismic refraction, The Sea 4-1, 53-84.
5. Geological Survey of Japan (2000). Gravity map CD-ROM of Japan, Digital Geoscience Map P-2.
6. Aoi, S. and H. Fujiwara (1999). 3d finite-difference method using discontinuous grids, Bull. Seism. Soc. Am. 89, 918-930.
7. Pitarka, A. (1999). 3d elastic finite-difference modeling of seismic motion using staggered grids with nonuniform spacing, Bull. Seism. Soc. Am., 89, 54-68.
8. Graves, R. W. (1996). Simulating seismic wave propagation in 3D elastic media using staggered-grid finite difference, Bull. Seism. Soc. Am. 86, 1091-1106.
9. Cejan, C., D. Kosloff, R. Kosloff, and M. Reshelf (1985). A nonreflecting boundary condition for discrete acoustic and elastic wave eqations, Geophysics 50, 706-708.
10. Ukawa, M. and Y. Fukao (1981). Poisson's ratios of the upper and lower crust and the sub-Moho mantle beneath central Honsu, Japan, Tectonophysics 77, 233-256.
11. Aoki, H, T. Toda, Y. Sasaki, T. Ooida, I. Muramatsu, and I. Furuya (1972). Crustal structure in the profile across central Japan as derived from explosion seismic observations, J. Phys. Earth, 20, 197-223.
12. Yamazaki, F., and T. Ooida (1985). Configuration of Subducted Philippine Sea Plate beneath the Cubu District, Central Japan., Zishin II, 38, 193-201 (In Japanese).
13. Neidell, N. S., and M. T. Tarner (1971). Semblance and other coherency measures for multichannnel data, Geophysics, 36, 482-497.
14. Geographical Survey Institute (1997). Digital map of 50m grid (Elevation), Japan, CD-ROM
15. Wessel, P., and W. H. F. Smith (1998). New, improved version of Generic Mapping Tool released, EOS, 79, 579.

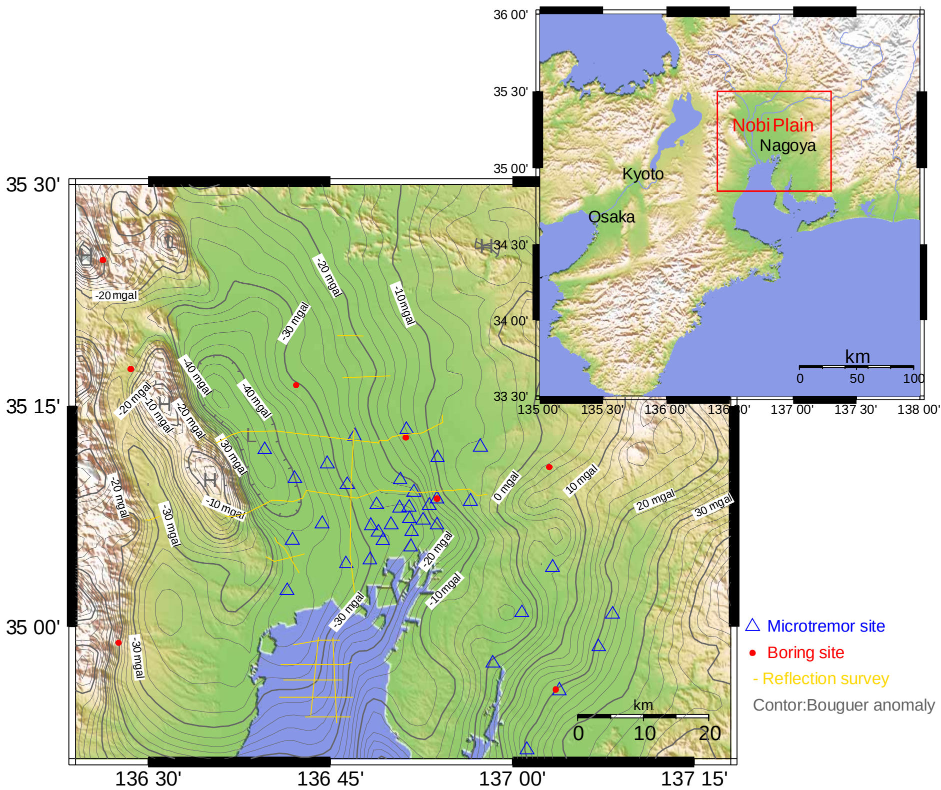

Figure 1. Location map of the Nobi plain and locations of the geophysical survey carried out in the Nobi plain. Yellow lines, blue open triangle, red solid circle and blue solid triangle denote refraction survey lines and microtremor observation sites PS logging sites. Contour shows gravity Bouguer anomaly by Geological Survey of Japan [3]

.

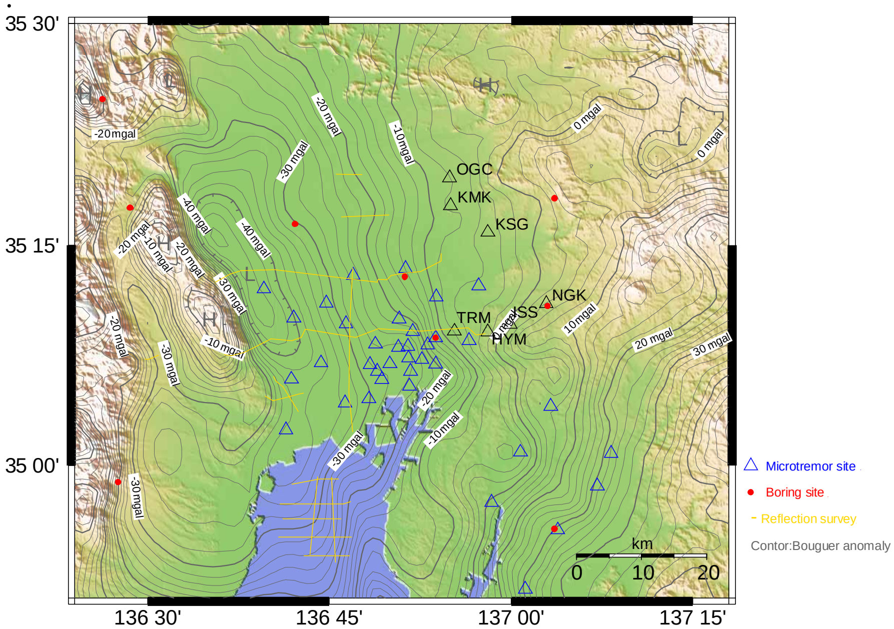

Figure 2. Locations of microtremor exploration sites.

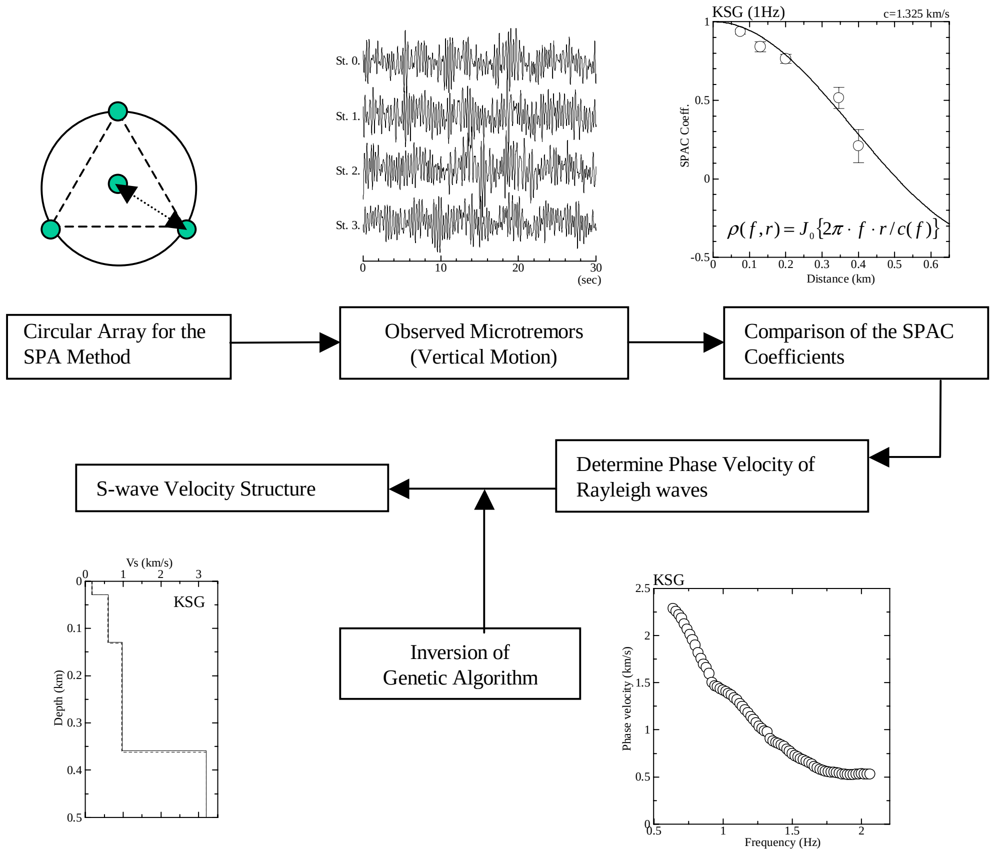

Figure 3. A flow of observation and analysis in the SPAC method for estimating S-wave velocity structures using microtremor explorations.

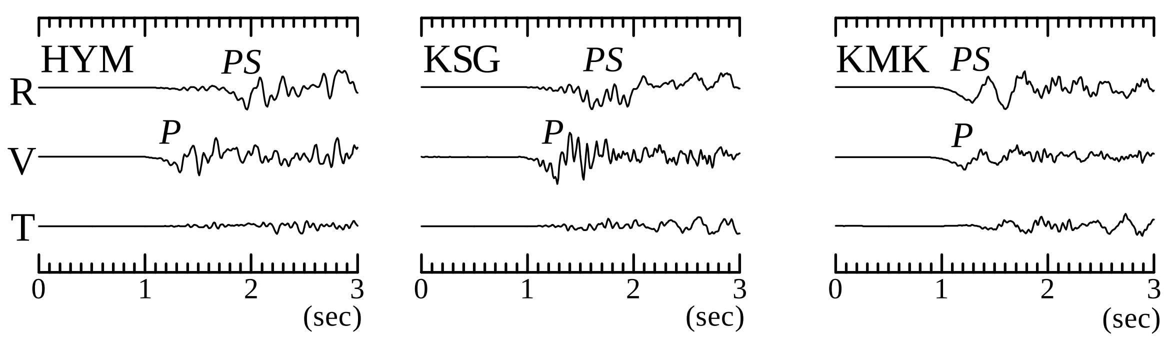

Figure 4. Examples of observed velocity waveforms of P-wave portion during M5.5 event at HYM, KSG and KMK. R, V and T denote Radial, Vertical and Transverse component, respectively.

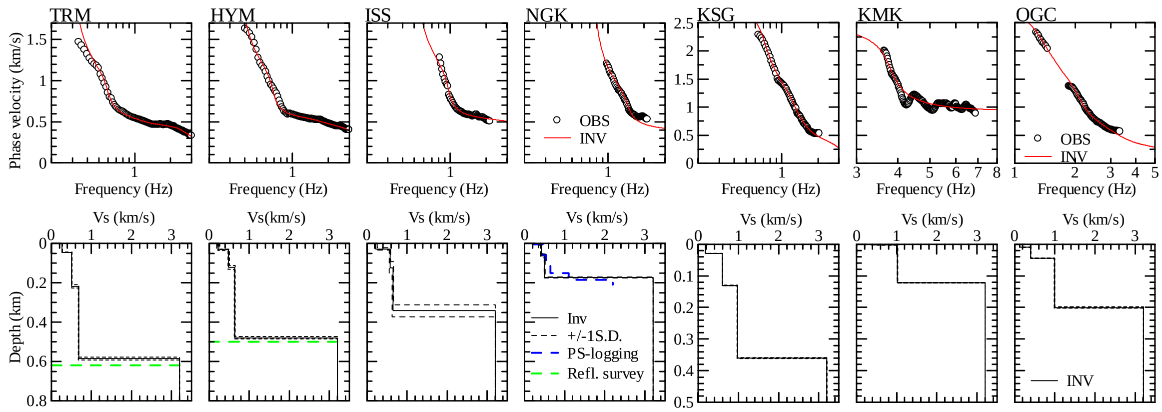

Figure 5. Phase velocities and S-wave structures obtained by mictoremor explorations.

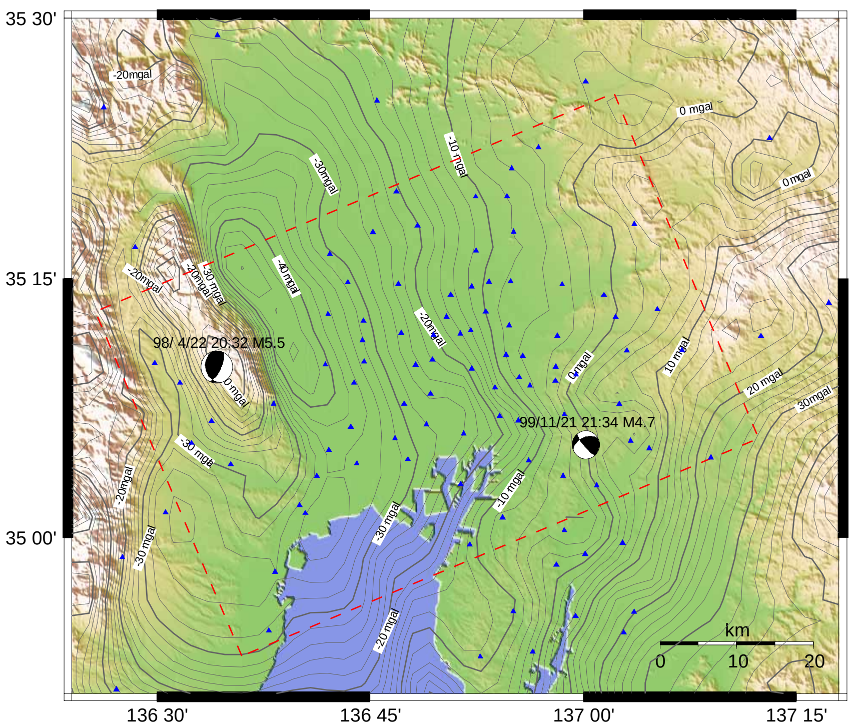

Figure 6. Modeled area and epicenters of M5.5 and M4.7 event.

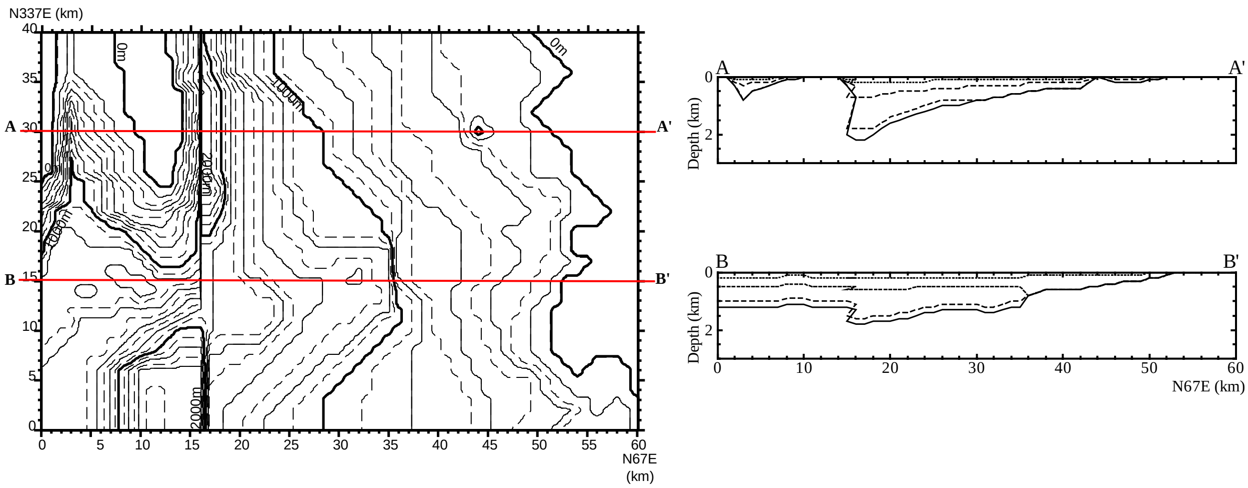

Figure 7. Depth contour of the basement and cross section to the depth of 2.5 km across A-A' and B-B' line.

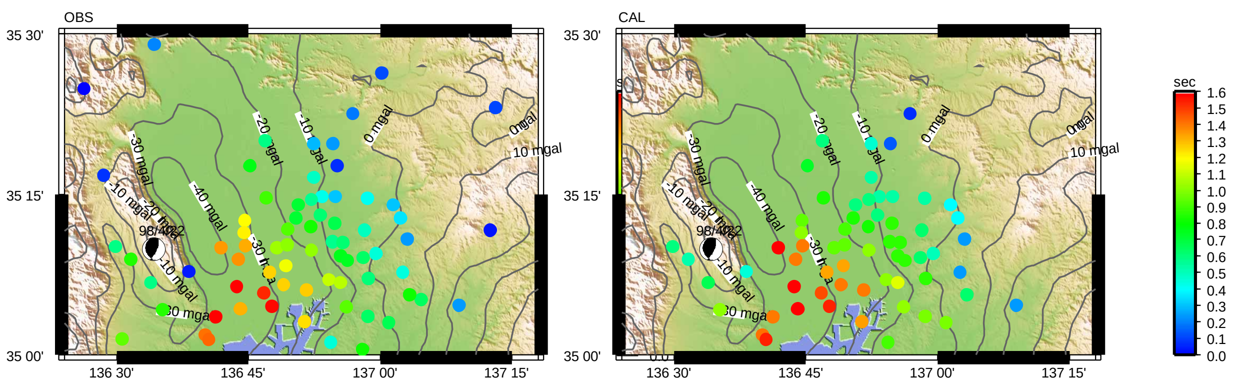

Figure 8. PS-P time distribution. (a) Observation and (b) calculated using the model constructed in this study.

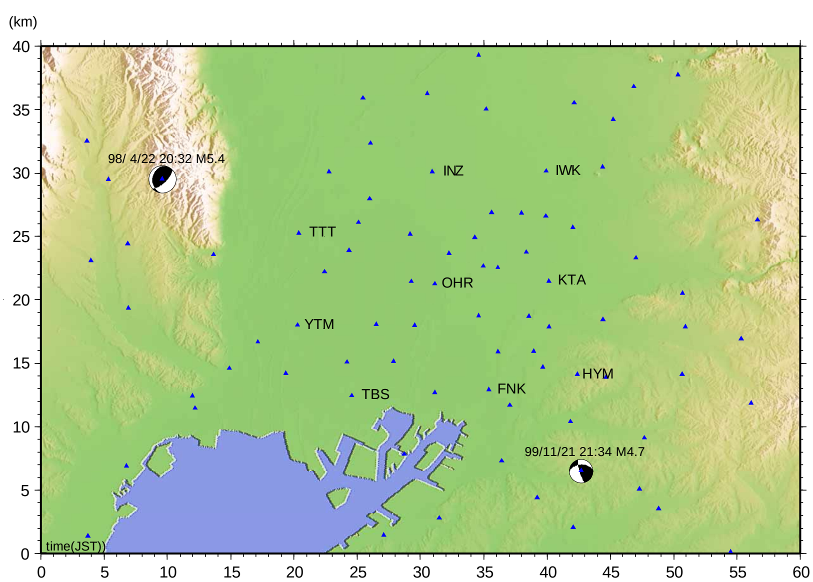

Figure 9. Map of seismic observation sites used in this study

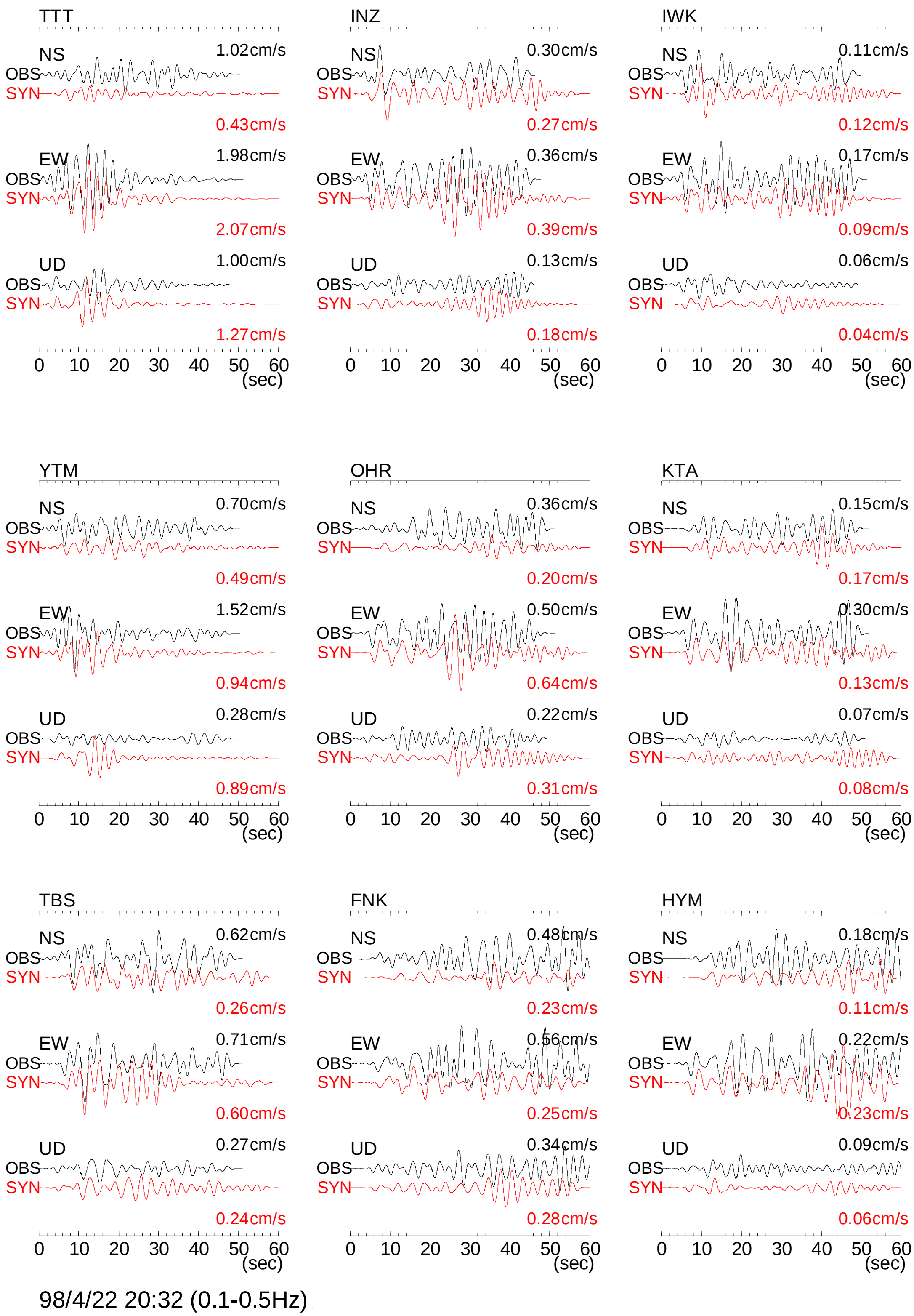

Figure 10. Examples of bandpass filtered (0.1-0.5Hz) velocity seismograms at 9 sites during M5.5 event. Location of each site is shown in fig.9.

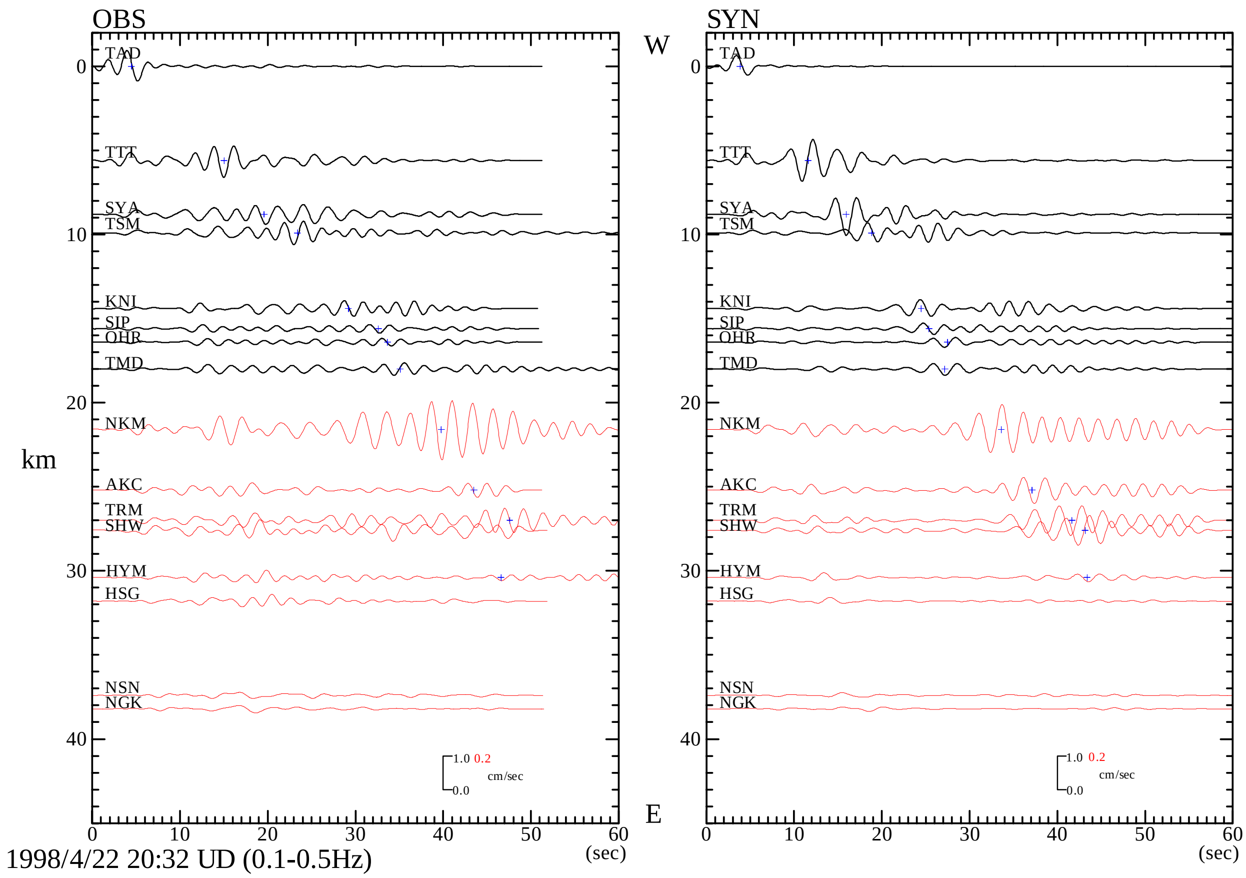

Figure 11. Bandpass filtered (0.1-0.5Hz) velocity seismograms (UD comp.) for the sites along EW direction from the source. Blue plus denote maximum part of the envelope of the phase.

Figure12. Examples of bandpass filtered (0.1-0.5Hz) velocity seismograms at 9 sites during M4.7 event. Location of each site is shown in fig.9.

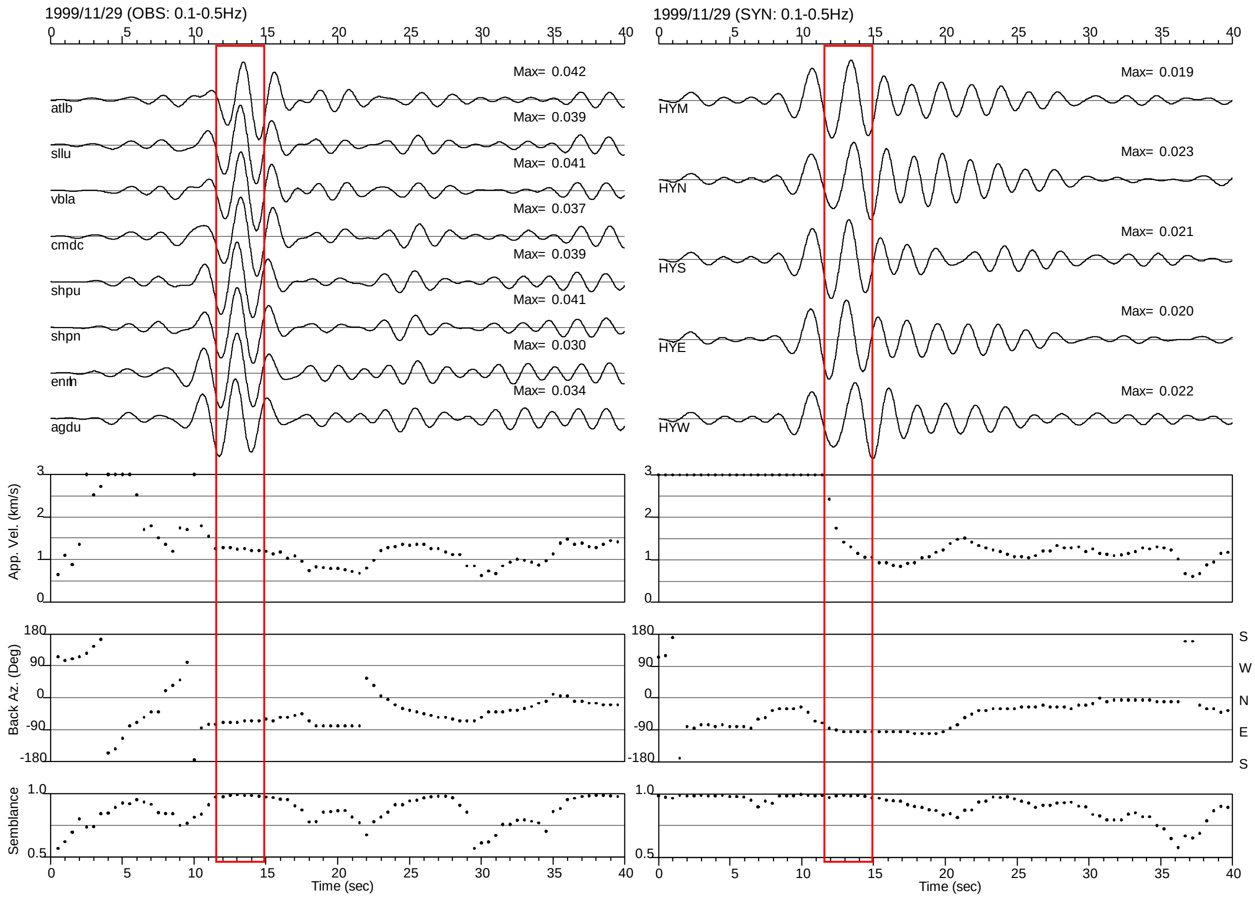

Figure13. Apparent velocities, arrival directions and semblance values obtained from semblance analysis of the vertical component on (a) observed and (b) synthetic seismograms. Arrival directions are measured in degree anti-clock wise from north. Rayleigh wave propagation is seen in the red rectangler.

Table 1. Array size of microtremor explorations at each site.

	ISS	NGK	KSG	KMK	OGC
S (m)	75	75	75	40	50
M (m)	200	150	200	75	125
L (m)	500	400	400	150	300

Table 2. Geophysical parameters of the each sedimentary layers of the Nobi plain. Depth means upper boundary of the each layer.

Depth (km)	Vp (km/s)	Vs (km/s)	Rho (g/cm3)	Q*
0.0	1.8	0.3	1.8	30
Variable	2.0	0.6	2,1	60
Variable	2.2	0.9	2.2	80
Variable	3.2	1.4	2.3	100

* Assumed value

Table 3. Geophysical parameters of the surrounding crustal model.

Depth (km)	Vp (km/s)	Vs (km/s)	Rho (g/cm3)	Q*
Variable	5.5	3.2	2.8	250
4.0	6.0	3.6	2.9	300
24.0	6.6	3.8	3.0	300
29.0	7.8	4.4	3.2	500
Variable	8.2	4.6	3.4	900

* Assumed value